

---

# MODAN-MULSUPCON: MODALITY- AND ANATOMY-AWARE MULTI-LABEL SUPERVISED CONTRASTIVE PRETRAINING FOR MEDICAL IMAGING

---

**Eichi Takaya**

AI Lab  
Tohoku University Hospital  
Miyagi, Japan  
eichi.takaya.d5@tohoku.ac.jp

**Ryusei Inamori**

Department of Diagnostic Imaging  
Tohoku University Graduate School of Medicine  
Miyagi, Japan

## ABSTRACT

**Background and objective:** Expert annotations limit large-scale supervised pretraining in medical imaging, while ubiquitous metadata (modality, anatomical region) remain underused. We introduce ModAn-MulSupCon, a modality- and anatomy-aware multi-label supervised contrastive pretraining method that leverages such metadata to learn transferable representations.

**Method:** Each image’s modality and anatomy are encoded as a multi-hot vector. A ResNet-18 encoder is pretrained on a mini subset of RadImageNet (miniRIN, 16,222 images) with a Jaccard-weighted multi-label supervised contrastive loss, and then evaluated by fine-tuning and linear probing on three binary classification tasks—ACL tear (knee MRI), lesion malignancy (breast ultrasound), and nodule malignancy (thyroid ultrasound).

**Result:** With fine-tuning, ModAn-MulSupCon achieved the best AUC on MRNet-ACL (0.964) and Thyroid (0.763), surpassing all baselines ( $p < 0.05$ ), and ranked second on Breast (0.926) behind SimCLR (0.940; not significant). With the encoder frozen, SimCLR/ImageNet were superior, indicating that ModAn-MulSupCon representations benefit most from task adaptation rather than linear separability.

**Conclusion:** Encoding readily available modality/anatomy metadata as multi-label targets provides a practical, scalable pretraining signal that improves downstream accuracy when fine-tuning is feasible. ModAn-MulSupCon is a strong initialization for label-scarce clinical settings, whereas SimCLR/ImageNet remain preferable for frozen-encoder deployments.

**Keywords** Medical imaging · Supervised contrastive learning · Multi-label learning

## 1 Introduction

In recent years, self-supervised learning (SSL) has rapidly gained traction in medical imaging [1][2]. The primary reason is the substantial cost and effort required from clinical experts for annotation, which makes large-scale supervised pretraining difficult to scale. Although hospital PACS archives contain vast amounts of unlabeled images, much of this data has remained unused. To bridge this gap, label-free self-supervised pretraining has attracted increasing attention.

Prior work on SSL for medical imaging has explored a variety of approaches, including pretext tasks such as jigsaw puzzles [3], contrastive-learning methods [4], and masked-autoencoder-based techniques [5]. However, pretraining strategies that explicitly leverage large datasets spanning multiple modalities and anatomical regions remain underexplored. While large datasets for pretraining such as RadImageNet [6] are becoming available, methods that exploit them have largely been limited to supervised learning with disease labels or simple MAE-style objectives [6][7].

In this study, we propose a pretraining method that exploits two medical-image-specific yet easily obtainable attributes: modality and anatomical region. These attributes can be acquired for virtually any medical image without specialist annotation, making them highly scalable.

Our approach encodes each image’s modality and anatomical region as independent one-hot vectors, concatenates them into a multi-hot label, and performs pretraining with a distance-aware loss using this target. This enables the encoder to learn representations that reflect modality-specific physics and anatomical structure, which in turn can improve both the efficiency of fine-tuning and downstream accuracy.

## 2 Related Works

### 2.1 Self-Supervised Learning (SSL) in Medical Imaging

Early SSL for medical imaging primarily relied on pretext tasks such as rotation prediction and jigsaw puzzles [8][3]. Since 2020, however, contrastive learning has been introduced: adaptations of SimCLR [9] and MoCo [10] to medical images have demonstrated strong performance and data efficiency [11][12]. These methods treat alternative slices from the same study or augmented views as positives, while maintaining large queues of negatives to learn robust representations.

Multi-modal contrastive approaches that couple images with text have also been actively studied. Using report-paired X-rays, methods such as GLoRIA [13] and BioViL [14] jointly optimize global and local image–text alignment and achieve strong transfer even with limited labels. More recently, masked image modeling (MIM) has come to the fore as a pretraining paradigm for Transformer-based networks [15][16][17]. Because MIM can be trained with a single reconstruction objective, it is easy to implement, and has been extended to 3D volumes [18] and temporal sequences [19], as well as combined with contrastive learning in multitask pretraining [20].

Despite recent progress, SSL pretraining on large public datasets (e.g., RadImageNet) has mostly relied on disease-label supervision [6] or simple MAE baselines [7] and has not explicitly leveraged hierarchical metadata such as modality or body part.

### 2.2 Learning with Multi-Label Targets

Multi-label learning seeks to predict multiple labels for a single input. Classical approaches include problem-transformation methods such as Binary Relevance [21] and Label Powerset [22], as well as algorithm-adaptation methods exemplified by ML-KNN [23] and Rank-SVM [24].

With the rise of deep learning, many studies have modeled label dependencies within the network. For example, CNN–RNN architectures [25] learn label co-occurrence patterns. Spatial Regularization Networks [26] represent inter-label dependencies with attention maps. ML-GCN [27] leverages graph convolution over label graphs to improve accuracy on benchmarks such as MS-COCO. In extreme multi-label text classification, tree-based methods such as AttentionXML [28] achieve both speed and high accuracy on corpora like Amazon-3M.

Methods for hierarchical multi-label prediction have also been proposed. However, many are restricted to single-path trees [29][30]. As an alternative, representing labels as multi-hot vectors has been shown to be effective [31].

Multi-label problem settings are common in medical imaging. In chest X-rays (e.g., CheXpert [32], MIMIC-CXR [33]), multiple conditions such as pneumonia and pneumothorax must be predicted simultaneously. Recent state-of-the-art models combine CNN backbones with GCNs or supervised contrastive losses to capture label co-occurrence [34][35][27].

Our method represents the two meta-labels (modality and anatomy) as separate one-hot vectors and learns from their concatenation as a multi-hot target. It is closest to Binary Relevance (it avoids class explosion as the number of labels grows), yet remains compatible with deep learning in that a single shared network learns the representation. Accordingly, our approach can be viewed as Binary Relevance extended with hierarchical metadata within a supervised contrastive framework.

## 3 Method

### 3.1 Modality- and Anatomy-Aware Multi-Label Supervised Contrastive Learning (ModAn-MulSupCon)

Figure 1 provides an overview of the proposed ModAn-MulSupCon. For an arbitrary collection of medical images:

1. Map an input image  $X$  with the encoder  $f_\theta(\cdot)$  to a  $d$ -dimensional feature vector  $\mathbf{z}$ .
2. Encode the image *metadata* (modality and anatomical region) as a  $k$ -dimensional multi-hot label  $\mathbf{y} \in \{0, 1\}^k$ .
3. Train  $f_\theta$  with a multi-label contrastive loss.

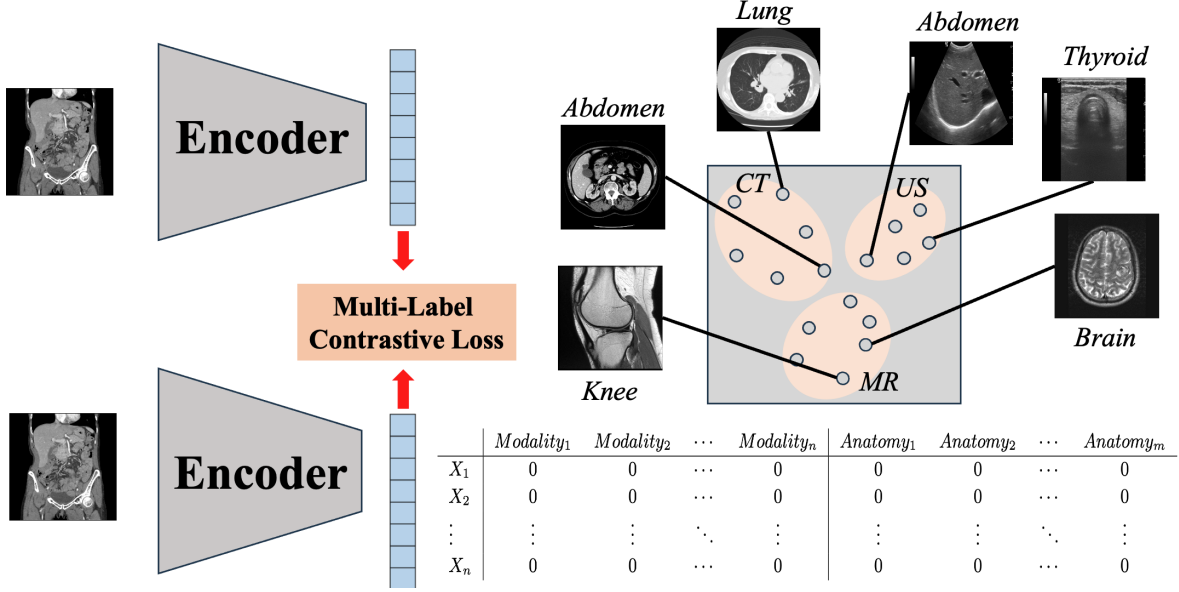


Figure 1: ModAn-MulSupCon: a shared encoder maps images to embeddings trained with a Jaccard-weighted multi-label supervised contrastive loss (Eq. 3). Metadata are encoded as a multi-hot vector (modality+anatomy), encouraging modality-aware clusters (CT/US/MR) and anatomical coherence (lung, abdomen, thyroid, brain, knee).

The pretrained encoder can subsequently be fine-tuned for tasks such as classification, detection, and segmentation.

### 3.2 Multi-Label Contrastive Loss

To pretrain the encoder, we minimize a multi-label supervised contrastive loss.

We first recall the InfoNCE loss for an anchor view  $a$  and its positive view  $p^*$  (two augmentations of the same image) [36]:

$$\mathcal{L}_{\text{InfoNCE}} = -\log \frac{\exp(\mathbf{z}_a^\top \mathbf{z}_{p^*}/T)}{\sum_{k \in A(a)} \exp(\mathbf{z}_a^\top \mathbf{z}_k/T)}. \quad (1)$$

Here  $\mathbf{z}_i \in \mathbb{R}^d$  denotes the  $\ell_2$ -normalized representation of view  $i$ ,  $T > 0$  is the temperature, and  $A(a)$  is the set of all in-batch views excluding the anchor, i.e.,  $A(a) = \{1, \dots, 2N\} \setminus \{a\}$  (two views per image in a batch of  $N$  images).

If each image is associated with an explicit class label  $y_i$ , the positive set for anchor  $a$  is

$$P(a) = \{p \in A(a) \mid y_p = y_a\},$$

and the supervised contrastive loss is [37]

$$\mathcal{L}_{\text{SupCon}} = -\frac{1}{|P(a)|} \sum_{p \in P(a)} \log \frac{\exp(\mathbf{z}_a^\top \mathbf{z}_p/T)}{\sum_{k \in A(a)} \exp(\mathbf{z}_a^\top \mathbf{z}_k/T)}. \quad (2)$$

In the multi-label setting, following prior work, each image  $i$  is annotated with a binary vector  $\mathbf{y}_i \in \{0, 1\}^k$  indicating the presence of  $k$  attributes (e.g., modality and anatomy). To account for partial matches between label sets, pairwise contributions are weighted by the Jaccard similarity [38]:

$$w_{ap} = \text{Jaccard}(\mathbf{y}_a, \mathbf{y}_p) = \frac{|S(a) \cap S(p)|}{|S(a) \cup S(p)|} \in [0, 1],$$

where  $S(i) = \{m \mid (\mathbf{y}_i)_m = 1\}$  is the set of active labels for sample  $i$ . Samples whose label similarity is at least a threshold  $\tau \in [0, 1]$  are treated as positives:

$$P_\tau(a) = \{p \in A(a) \mid w_{ap} \geq \tau\}.$$

The resulting multi-label supervised contrastive objective is

$$\mathcal{L}_{\text{MulSupCon}} = -\frac{1}{|P_{\tau}(a)|} \sum_{p \in P_{\tau}(a)} w_{ap} \log \frac{\exp(\mathbf{z}_a^{\top} \mathbf{z}_p / T)}{\sum_{k \in A(a)} \exp(\mathbf{z}_a^{\top} \mathbf{z}_k / T)}, \quad (3)$$

which is known as the Multi-Label Supervised Contrastive Loss [38].

## 4 Experiments

### 4.1 Datasets

#### 4.1.1 Pretraining Dataset

RadImageNet (RIN) [6] provides modality and anatomical metadata together with a large number of cases. RIN contains approximately 1.3 M medical images annotated with 165 disease and normal classes.

However, using the full dataset would require tens of GPU-days per run, which is undesirable from the perspective of reproducibility and design exploration. Therefore, we randomly sampled up to 100 images per class from the 165 classes in RIN (using all images for classes with fewer than 100 cases) to construct the subset miniRIN. As a result, miniRIN comprises 16 222 images in total.

#### 4.1.2 Downstream Dataset

To evaluate the transferability of encoders trained on miniRIN, we selected three publicly available datasets with relatively few cases (Table 1), each being a binary classification task.

Table 1: Downstream datasets used for transfer-learning evaluation.

Dataset	Modality	Task (binary)	Images (class distribution)	Source
Thyroid US	Ultrasound	Benign vs. malignant nodule	349 (288/61)	[39]
Breast US	Ultrasound	Benign vs. malignant lesion	779 (569/210)	[40]
MRNet-ACL	Knee MRI	ACL tear vs. intact ligament	1021 (569/452)	[41]

### 4.2 Experimental Setting

In this study, we compared five initialization settings, with primary emphasis on classifiers fine-tuned from the proposed ModAn-MulSupCon pretraining model:

1. ModAn-MulSupCon (proposed)
2. miniRIN SimCLR pretrained model (miniRINSimCLR)
3. 165-class supervised classifier trained on miniRIN (miniRIN165)
4. ImageNet-pretrained model (ImageNet)
5. Random initialization (Scratch).

For each setting, we performed both fine-tuning (updating all layers) and linear probing (training only a linear classifier with the encoder frozen) on three downstream tasks, and evaluated performance using AUC.

**Data splits and repetitions.** All methods were evaluated on the same fixed 5-fold partition for each downstream dataset. To characterize variance arising from training stochasticity - primarily mini-batch sampling - we repeated the entire 5-fold training/evaluation procedure ten times while keeping the data splits unchanged. In each repeat, models were trained/evaluated on all five folds and the fold-wise AUCs were averaged to obtain a single summary value. Thus, each method yielded ten summary AUCs, which were used for paired comparisons via the Wilcoxon signed-rank test (two-sided,  $\alpha = 0.05$ ).

Table 2: Pretraining configurations across initialization settings. Common augmentations: RandomResizedCrop, RandomHorizontalFlip, ColorJitter ( $p=0.8$ ), and RandomGrayscale ( $p=0.2$ ).

Method	Loss / Init.	Temp. $T$	$\tau$	Optimizer (lr, mom / wd)	Epochs	Batch
ModAn-MulSupCon	Multi-label SupCon	0.07	0.3	SGD (0.05, 0.9 / $10^{-4}$ )	1000	256
miniRINSimCLR	NT-Xent	0.10	–	SGD (0.05, 0.9 / $10^{-4}$ )	1000	256
miniRIN165	Cross-entropy	–	–	Adam (default)	1000	256
ImageNet	Off-the-shelf	–	–	–	–	–
Scratch	–	–	–	–	–	–

Table 3: Hyperparameters for downstream fine-tuning and linear probing (common across tasks).

Epochs	Batch size	Optimizer	LR scheduler
10	32	Adam ( $1 \times 10^{-4}$ )	StepLR(5, $\gamma=0.1$ )

**Representation visualization.** For qualitative analysis, we visualized learned representations from each encoder. Specifically, we extracted the penultimate feature vectors. These vectors were embedded into two dimensions using UMAP (Uniform Manifold Approximation and Projection) [42]. To focus on pretraining effects, we visualized the miniRIN training set itself; for ImageNet and Scratch, features were computed on the same miniRIN training images for comparability, with no downstream or test images included.

### 4.3 Implementation Details

We used ResNet-18 as the backbone and modified the first convolution to accept a single-channel input (kernel  $3 \times 3$ , stride 1), while keeping the remaining layers unchanged. During contrastive pretraining, we adopted a SimCLR-style TwoCropTransform: each image is augmented into two views using RandomResizedCrop with scale  $[0.2, 1.0]$ , RandomHorizontalFlip, ColorJitter (applied with probability 0.8), and RandomGrayscale (applied with probability 0.2).

Pretraining configurations for all initializations are summarized in Table 2. In brief, ModAn-MulSupCon uses a multi-label supervised contrastive loss with temperature  $T=0.07$  and threshold  $\tau=0.3$ , optimized by SGD (learning rate 0.05, momentum 0.9, weight decay  $10^{-4}$ ) for 1000 epochs with batch size 256. The miniRINSimCLR baseline uses NT-Xent with  $T=0.10$  under the same optimizer and schedule, and the miniRIN165 supervised baseline is trained with cross-entropy using Adam (default settings). ImageNet and Scratch correspond to off-the-shelf ImageNet weights and random initialization, respectively.

For downstream evaluation, we applied a single training recipe to both fine-tuning (all layers trainable) and linear probing (encoder frozen and only a linear classifier trained). As shown in Table 3, we trained for 10 epochs with batch size 32 using Adam (learning rate  $1 \times 10^{-4}$ ) and a StepLR scheduler (decay at epoch 5 with factor  $\gamma=0.1$ ).

All implementations were in PyTorch 2.1.2, and experiments were run on a single NVIDIA Quadro RTX 8000 (48 GB) GPU.

### 4.4 Results

Under fine-tuning, ModAn-MulSupCon achieved the best AUC on both ACL and Thyroid (Table 4), surpassing all baselines ( $p < 0.05$  in both tasks). For Breast, miniRINSimCLR yielded a slightly higher AUC.

By contrast, with the linear probing, miniRINSimCLR and ImageNet performed best on ACL and Breast, while the ModAn-MulSupCon yielded the lowest scores (Table 5). On Thyroid, miniRINSimCLR was best; ModAn-MulSupCon was significantly better than Scratch only.

The wall-clock per-epoch times were approximately 10 min/epoch for pretraining, 0.7 sec/epoch for fine-tuning, and 0.1 sec/epoch for linear probing.

Figure 2 visualizes the learned embeddings with UMAP. Each point is colored by the combined metadata (modality+anatomy): we assign an arbitrary but fixed color to each (modality, anatomy) pair and use the same mapping across panels; the colors are nominal only and do not encode similarity, density, or frequency.

Table 4: Mean AUC and  $p$ -values (Wilcoxon signed-rank) after fine-tuning with  $10 \times 5$ -fold CV, comparing each baseline to the proposed SSL. Best AUCs are **boldfaced**, and  $p \leq 0.05$  is also **boldfaced**.

Pretraining	ACL		Breast		Thyroid	
	AUC	$p$ -value	AUC	$p$ -value	AUC	$p$ -value
ModAn-MulSupCon	<b>0.964</b>	–	0.926	–	<b>0.763</b>	–
miniRINSimCLR	0.951	< <b>0.05</b>	<b>0.940</b>	1.000	0.685	< <b>0.05</b>
miniRIN165	0.630	< <b>0.05</b>	0.666	< <b>0.05</b>	0.558	< <b>0.05</b>
ImageNet	0.876	< <b>0.05</b>	0.884	< <b>0.05</b>	0.696	< <b>0.05</b>
Scratch	0.907	< <b>0.05</b>	0.884	< <b>0.05</b>	0.677	< <b>0.05</b>

Table 5: Mean AUC and  $p$ -values for linear probing (pretrained encoder frozen; linear classifier only). Notation follows Table 4.

Pretraining	ACL		Breast		Thyroid	
	AUC	$p$ -value	AUC	$p$ -value	AUC	$p$ -value
ModAn-MulSupCon	0.681	–	0.717	–	0.639	–
miniRINSimCLR	<b>0.844</b>	1.000	<b>0.805</b>	1.000	<b>0.657</b>	0.935
miniRIN165	0.796	1.000	0.723	0.986	0.630	0.188
ImageNet	0.824	1.000	0.781	1.000	0.609	0.080
Scratch	0.697	0.999	0.724	0.999	0.557	< <b>0.05</b>

## 5 Discussion

We evaluated two regimes: full fine-tuning of the pretrained encoder and linear probing with the encoder frozen. Under fine-tuning, the ModAn-MulSupCon achieved the best AUC on both ACL (0.964) and Thyroid (0.763), and ranked second on Breast (0.926; the best was miniRINSimCLR at 0.940) (Table 4). By contrast, in linear probing, miniRIN-SimCLR and ImageNet were consistently superior, and the ModAn-MulSupCon lagged behind on all three tasks (e.g., ACL: 0.681 vs. 0.844 for SimCLR; Table 5). These results suggest that the ModAn-MulSupCon learns representations whose strength lies less in linear separability under freezing and more in their plasticity for task adaptation through fine-tuning. In practice, it is therefore best viewed as an initialization tailored for scenarios that assume fine-tuning.

ModAn-MulSupCon supervises the encoder with a multi-hot metadata target formed by concatenating modality and anatomy, and it weights pairwise terms by the Jaccard similarity (Eq. 3, Fig. 1). This weighting treats different yet related meta-attributes as “soft positives,” embedding hierarchical proximity into the representation space. As a result, the model learns non-linear features aligned with modality-specific physics and anatomical structure, which can be efficiently shaped into task boundaries during fine-tuning. Notably, this strong inductive bias enabled competitive transfer even with only miniRIN (16,222 images) for pretraining, and on some tasks it surpassed ImageNet-pretrained baselines.

As a complement, UMAP visualizations (Figure 2) show that both the ModAn-MulSupCon and SimCLR form clusters roughly organized by modality and anatomy. Whereas SimCLR exhibits higher linear separability when the encoder is frozen, the ModAn-MulSupCon yields more entangled clusters that nonetheless translate into superior accuracy after fine-tuning. This pattern is consistent with the fine-tuning advantage and frozen-encoder disadvantage observed in Tables 4 and 5.

On Breast (ultrasound), SimCLR achieved a slightly higher AUC (0.940) than the ModAn-MulSupCon (0.926) (Table 4). Ultrasound is strongly affected by device variability, speckle noise, and acquisition protocols; thus, coarse metadata such as modality and anatomy may be insufficient to constrain differences arising from subtle peri-lesional textures or ROI selection. In such cases, instance-level relational learning (e.g., SimCLR) can be advantageous for both linear separability under freezing and certain fine-tuned settings. This observation indicates that a metadata-driven inductive bias is not universally optimal; domains with high acquisition heterogeneity may benefit from finer-grained metadata (e.g., device or probe type) or from hybridizing metadata supervision with instance contrastive learning.

From an operational standpoint, SimCLR or ImageNet is preferable when the encoder must remain frozen for lightweight deployment. When full fine-tuning is feasible, the ModAn-MulSupCon is more likely to deliver superior final performance. A practical guideline, therefore, is: use SimCLR/ImageNet for frozen encoders, and adopt the ModAn-MulSupCon when fine-tuning is possible.

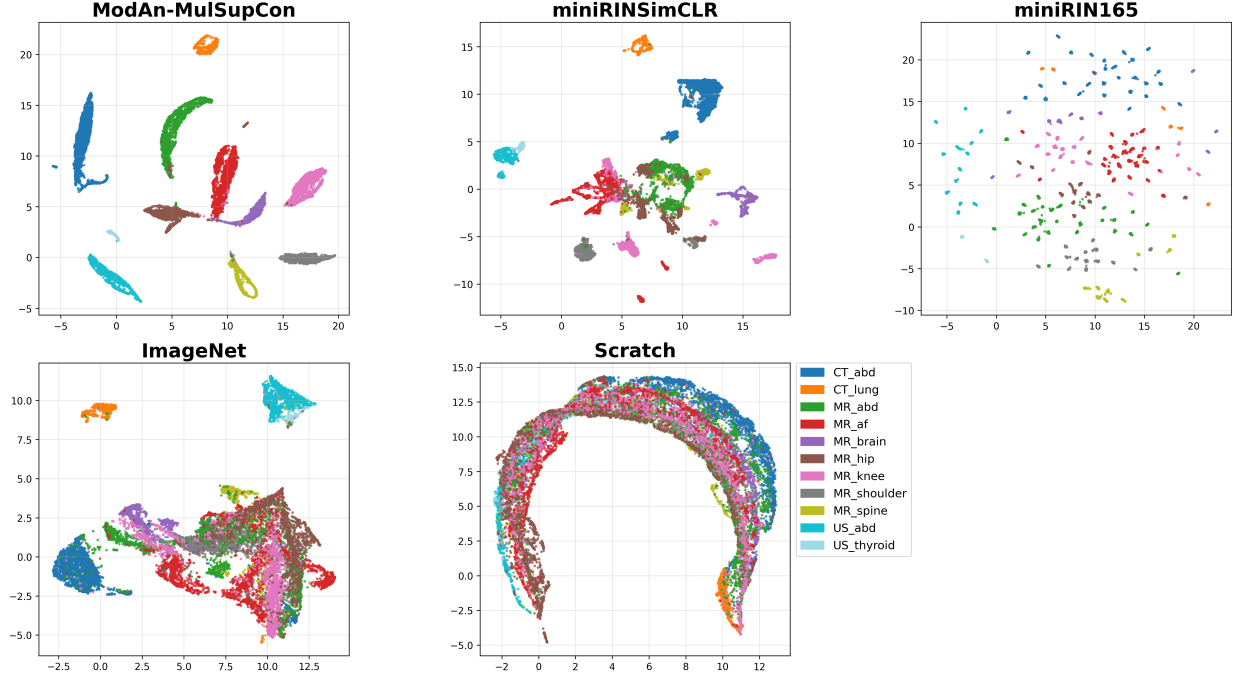


Figure 2: UMAP projections of penultimate-layer embeddings from five initializations— ModAn-MulSupCon, miniRIN-SimCLR, ImageNet, miniRIN-165, and Scratch. Each point is colored by the combined metadata (modality+anatomy): we assign an arbitrary but fixed color to each (modality, anatomy) pair and use the same mapping across panels; the colors are nominal only and do not encode similarity, density, or frequency.

This study has several limitations. First, the scalability assessment is limited to the miniRIN scale. Second, the downstream datasets offer restricted modality diversity, leaving untested regions. Third, our evaluation assumes a ResNet-18 backbone; extensions to ViT-style architectures and 3D backbones are needed.

## 6 Conclusion

We introduced ModAn-MulSupCon, a modality- and anatomy-aware multi-label supervised contrastive pretraining approach that turns readily available metadata into a useful supervision signal. In transfer, it performs best when the encoder can be fully fine-tuned, whereas generic pretraining such as SimCLR or ImageNet is preferable when the encoder must remain frozen. In practice, we recommend ModAn-MulSupCon for scenarios that permit fine-tuning and generic pretraining for deployments that require a frozen encoder. Because modality and anatomy labels are broadly available without expert annotation, the proposed strategy offers an immediately deployable, label-efficient pretraining signal for clinical pipelines operating under limited annotations.

Looking ahead, we will scale pretraining beyond miniRIN, enrich the metadata used for supervision with factors such as device or probe type, view, and laterality, integrate metadata supervision with instance-level contrastive objectives, evaluate additional backbones including Vision Transformers and three-dimensional encoders, and assess robustness across institutions and modalities while expanding to broader clinical classification settings.

## Acknowledgments

This work was supported by JSPS KAKENHI Grant Number JP24K15174.

## References

- [1] Tobias Uelwer, Jan Robine, Stefan Sylvius Wagner, Marc Höftmann, Eric Upschulte, Sebastian Konietzny, Maike Behrendt, and Stefan Harmeling. A survey on self-supervised methods for visual representation learning. *Ma-*

- chine Learning*, 114(4):1–56, 2025. Publisher: Springer.
- [2] Veenu Rani, Munish Kumar, Aastha Gupta, Monika Sachdeva, Ajay Mittal, and Krishan Kumar. Self-supervised learning for medical image analysis: a comprehensive review. *Evolving Systems*, 15(4):1607–1633, 2024. Publisher: Springer.
- [3] Keisuke Sugawara, Eichi Takaya, Ryusei Inamori, Yuma Konaka, Jumpei Sato, Yuta Shiratori, Fumihito Hario, Tomoya Kobayashi, Takuya Ueda, and Yoshikazu Okamoto. Breast cancer classification based on breast tissue structures using the Jigsaw puzzle task in self-supervised learning. *Radiological Physics and Technology*, pages 1–10, 2025. Publisher: Springer.
- [4] Yawen Wu, Dewen Zeng, Zhepeng Wang, Yiyu Shi, and Jingtong Hu. Distributed contrastive learning for medical image segmentation. *Medical Image Analysis*, 81:102564, 2022. Publisher: Elsevier.
- [5] Jiabin Zhuang, Linshan Wu, Qiong Wang, Peng Fei, Varut Vardhanabhuti, Lin Luo, and Hao Chen. Mim: Mask in mask self-supervised pre-training for 3d medical image analysis. *IEEE Transactions on Medical Imaging*, 2025. Publisher: IEEE.
- [6] Xueyan Mei, Zelong Liu, Philip M. Robson, Brett Marinelli, Mingqian Huang, Amish Doshi, Adam Jacobi, Chendi Cao, Katherine E. Link, Thomas Yang, Ying Wang, Hayit Greenspan, Timothy Deyer, Zahi A. Fayad, and Yang Yang. RadImageNet: An Open Radiologic Deep Learning Research Dataset for Effective Transfer Learning. *Radiology: Artificial Intelligence*, 4(5):e210315, September 2022.
- [7] Zelong Liu, Andrew Tieu, Nikhil Patel, George Soutanidis, Louisa Deyer, Ying Wang, Sean Huver, Alexander Zhou, Yunhao Mei, Zahi A Fayad, et al. Vis-mae: An efficient self-supervised learning approach on medical image segmentation and classification. In *International Workshop on Machine Learning in Medical Imaging*, pages 95–107. Springer, 2024.
- [8] Xiaomeng Li, Xiaowei Hu, Xiaojuan Qi, Lequan Yu, Wei Zhao, Pheng-Ann Heng, and Lei Xing. Rotation-oriented collaborative self-supervised learning for retinal disease diagnosis. *IEEE Transactions on Medical Imaging*, 40(9):2284–2294, 2021. Publisher: IEEE.
- [9] Ting Chen, Simon Kornblith, Mohammad Norouzi, and Geoffrey Hinton. A simple framework for contrastive learning of visual representations. In *International conference on machine learning*, pages 1597–1607. PmLR, 2020.
- [10] Kaiming He, Haoqi Fan, Yuxin Wu, Saining Xie, and Ross Girshick. Momentum contrast for unsupervised visual representation learning. In *Proceedings of the IEEE/CVF conference on computer vision and pattern recognition*, pages 9729–9738, 2020.
- [11] Zeyu Ren, Xiangyu Kong, Yudong Zhang, and Shuihua Wang. UKSSL: Underlying knowledge based semi-supervised learning for medical image classification. *IEEE Open Journal of Engineering in Medicine and Biology*, 5:459–466, 2023. Publisher: IEEE.
- [12] Hari Sowrirajan, Jingbo Yang, Andrew Y Ng, and Pranav Rajpurkar. Moco pretraining improves representation and transferability of chest x-ray models. In *Medical Imaging with Deep Learning*, pages 728–744. PMLR, 2021.
- [13] Shih-Cheng Huang, Liye Shen, Matthew P Lungren, and Serena Yeung. Gloria: A multimodal global-local representation learning framework for label-efficient medical image recognition. In *Proceedings of the IEEE/CVF international conference on computer vision*, pages 3942–3951, 2021.
- [14] Benedikt Boecking, Naoto Usuyama, Shruthi Bannur, Daniel C Castro, Anton Schwaighofer, Stephanie Hyland, Maria Wetscherek, Tristan Naumann, Aditya Nori, Javier Alvarez-Valle, and others. Making the most of text semantics to improve biomedical vision–language processing. In *European conference on computer vision*, pages 1–21. Springer, 2022.
- [15] Lei Zhou, Huidong Liu, Joseph Bae, Junjun He, Dimitris Samaras, and Prateek Prasanna. Self pre-training with masked autoencoders for medical image classification and segmentation. In *2023 IEEE 20th International Symposium on Biomedical Imaging (ISBI)*, pages 1–6. IEEE, 2023.
- [16] Jiabin Zhuang, Luyang Luo, Qiong Wang, Mingxiang Wu, Lin Luo, and Hao Chen. Advancing Volumetric Medical Image Segmentation via Global-Local Masked Autoencoders. *IEEE Transactions on Medical Imaging*, 2025. Publisher: IEEE.
- [17] Zi’an Xu, Yin Dai, Fayu Liu, Weibing Chen, Yue Liu, Lifu Shi, Sheng Liu, and Yuhang Zhou. Swin MAE: masked autoencoders for small datasets. *Computers in biology and medicine*, 161:107037, 2023. Publisher: Elsevier.
- [18] Xin Yu, Qi Yang, Yinchu Zhou, Leon Y Cai, Riqiang Gao, Ho Hin Lee, Thomas Li, Shunxing Bao, Zhoubing Xu, Thomas A Lasko, and others. Unest: local spatial representation learning with hierarchical transformer for efficient medical segmentation. *Medical Image Analysis*, 90:102939, 2023. Publisher: Elsevier.



- [19] Lukas Buess, Marijn F Stollenga, David Schinz, Benedikt Wiestler, Jan Kirschke, Andreas Maier, Nassir Navab, and Matthias Keicher. Video-CT MAE: Self-supervised Video-CT Domain Adaptation for Vertebral Fracture Diagnosis. In *Medical Imaging with Deep Learning*, 2024.
- [20] Yucheng Tang, Dong Yang, Wenqi Li, Holger R Roth, Bennett Landman, Daguang Xu, Vishwesh Nath, and Ali Hatamizadeh. Self-supervised pre-training of swin transformers for 3d medical image analysis. In *Proceedings of the IEEE/CVF conference on computer vision and pattern recognition*, pages 20730–20740, 2022.
- [21] Grigorios Tsoumakas, Ioannis Katakis, and Ioannis Vlahavas. Mining multi-label data. *Data mining and knowledge discovery handbook*, pages 667–685, 2010. Publisher: Springer.
- [22] Matthew R Boutell, Jiebo Luo, Xipeng Shen, and Christopher M Brown. Learning multi-label scene classification. *Pattern recognition*, 37(9):1757–1771, 2004. Publisher: Elsevier.
- [23] Min-Ling Zhang and Zhi-Hua Zhou. ML-KNN: A lazy learning approach to multi-label learning. *Pattern recognition*, 40(7):2038–2048, 2007. Publisher: Elsevier.
- [24] André Elisseeff and Jason Weston. A kernel method for multi-labelled classification. *Advances in neural information processing systems*, 14, 2001.
- [25] Jiang Wang, Yi Yang, Junhua Mao, Zhiheng Huang, Chang Huang, and Wei Xu. Cnn-rnn: A unified framework for multi-label image classification. In *Proceedings of the IEEE conference on computer vision and pattern recognition*, pages 2285–2294, 2016.
- [26] Feng Zhu, Hongsheng Li, Wanli Ouyang, Nenghai Yu, and Xiaogang Wang. Learning spatial regularization with image-level supervisions for multi-label image classification. In *Proceedings of the IEEE conference on computer vision and pattern recognition*, pages 5513–5522, 2017.
- [27] Zhao-Min Chen, Xiu-Shen Wei, Peng Wang, and Yanwen Guo. Multi-label image recognition with graph convolutional networks. In *Proceedings of the IEEE/CVF conference on computer vision and pattern recognition*, pages 5177–5186, 2019.
- [28] Ronghui You, Zihan Zhang, Ziye Wang, Suyang Dai, Hiroshi Mamitsuka, and Shanfeng Zhu. Attentionxml: Label tree-based attention-aware deep model for high-performance extreme multi-label text classification. *Advances in neural information processing systems*, 32, 2019.
- [29] Shu Zhang, Ran Xu, Caiming Xiong, and Chetan Ramaiah. Use All The Labels: A Hierarchical Multi-Label Contrastive Learning Framework. In *2022 IEEE/CVF Conference on Computer Vision and Pattern Recognition (CVPR)*, pages 16639–16648, New Orleans, LA, USA, June 2022. IEEE.
- [30] Kiran Kokilepersaud, Seulgi Kim, Mohit Prabhushankar, and Ghassan AlRegib. Hex: Hierarchical emergence exploitation in self-supervised algorithms. In *2025 IEEE/CVF Winter Conference on Applications of Computer Vision (WACV)*, pages 1111–1121. IEEE, 2025.
- [31] Haixiang Li, Min Fang, Xiao Li, Bo Chen, and Guizhi Wang. Hierarchical multi-granular multi-label contrastive learning. *Pattern Recognition*, 164:111567, August 2025.
- [32] Jeremy Irvin, Pranav Rajpurkar, Michael Ko, Yifan Yu, Silvana Ciurea-Ilcus, Chris Chute, Henrik Marklund, Behzad Haghighi, Robyn Ball, Katie Shpanskaya, and others. Chexpert: A large chest radiograph dataset with uncertainty labels and expert comparison. In *Proceedings of the AAAI conference on artificial intelligence*, volume 33, pages 590–597, 2019. Issue: 01.
- [33] Alistair Johnson, Tom Pollard, Roger Mark, Seth Berkowitz, and Steven Horng. Mimic-cxr database. *PhysioNet10*, 13026:C2JT1Q, 2024.
- [34] Chengsheng Mao, Liang Yao, and Yuan Luo. Imagegcnn: Multi-relational image graph convolutional networks for disease identification with chest x-rays. *IEEE transactions on medical imaging*, 41(8):1990–2003, 2022. Publisher: IEEE.
- [35] Ajay Jaiswal, Tianhao Li, Cyprian Zander, Yan Han, Justin F Rousseau, Yifan Peng, and Ying Ding. Scalp-supervised contrastive learning for cardiopulmonary disease classification and localization in chest x-rays using patient metadata. In *2021 IEEE International Conference on Data Mining (ICDM)*, pages 1132–1137. IEEE, 2021.
- [36] Aaron van den Oord, Yazhe Li, and Oriol Vinyals. Representation learning with contrastive predictive coding. *arXiv preprint arXiv:1807.03748*, 2018.
- [37] Prannay Khosla, Piotr Teterwak, Chen Wang, Aaron Sarna, Yonglong Tian, Phillip Isola, Aaron Maschinot, Ce Liu, and Dilip Krishnan. Supervised contrastive learning. *Advances in neural information processing systems*, 33:18661–18673, 2020.

- [38] Vladimir Zaigrajew and Maciej Zieba. Contrastive learning for multi-label classification. In *Proceedings of Conference on Neural Information Processing Systems, New Orleans*, pages 1–8, 2022.
- [39] Lina Pedraza, Carlos Vargas, Fabián Narváez, Oscar Durán, Emma Muñoz, and Eduardo Romero. An open access thyroid ultrasound image database. In *10th International symposium on medical information processing and analysis*, volume 9287, pages 188–193. SPIE, 2015.
- [40] Walid Al-Dhabyani, Mohammed Gomaa, Hussien Khaled, and Aly Fahmy. Dataset of breast ultrasound images. *Data in brief*, 28:104863, 2020. Publisher: Elsevier.
- [41] Nicholas Bien, Pranav Rajpurkar, Robyn L Ball, Jeremy Irvin, Allison Park, Erik Jones, Michael Bereket, Bhavik N Patel, Kristen W Yeom, Katie Shpanskaya, and others. Deep-learning-assisted diagnosis for knee magnetic resonance imaging: development and retrospective validation of MRNet. *PLoS medicine*, 15(11):e1002699, 2018. Publisher: Public Library of Science San Francisco, CA USA.
- [42] Leland McInnes, John Healy, and James Melville. Umap: Uniform manifold approximation and projection for dimension reduction. *arXiv preprint arXiv:1802.03426*, 2018.